Biosensors and Bioelectronics 141 (2019) 111397

Contents lists available at ScienceDirect

Biosensors and Bioelectronics

journal homepage: www.elsevier.com/locate/bios

A catalytic molecule machine-driven biosensing method for amplified electrochemical detection of exosomes

Ya Cao[a], Lingling Li[a,b], Bing Han[a], Ying Wang[a], Yuhao Dai[a], Jing Zhao[a,*]

[a] Center for Molecular Recognition and Biosensing, School of Life Sciences, Shanghai University, 200444, PR China
[b] Shanghai Key Laboratory of Bio-Energy Crops, Shanghai University, 200444, PR China

ARTICLE INFO

Keywords:
Cascaded toehold-mediated strand displacement reaction
Catalytic molecule machine
Exosome detection
CD63
Click chemistry

ABSTRACT

Nowadays, exosomes that carry abundant information have attracted increasing attention as potent biomarkers of liquid biopsy and ideal candidates for early diagnosis and treatment of cancers. In this work, we propose a "principle-of-proof" biosensing method for amplified electrochemical detection of exosomes by using HepG2-derived exosomes as models. Specifically, target exosomes are enriched on anti-CD63-functionalized immunobeads and then recognized by a DNA chain containing CD63 aptamer region, which subsequently initiates a catalytic molecule machine that relies on cascade toehold-mediated strand displacement reaction. Benefiting from high efficiency of the molecule machine, the method shows a linear range from 1×10^5 to 5×10^7 particles/mL and a detection limit of 1.72×10^4 particles/mL toward target exosomes, better than most existing detection methods. Moreover, the method demonstrates a high specificity even in serum samples and suggests a potential use in clinic, which may provide sufficient information for disease diagnosis, especially early detection and prognosis monitoring of tumors.

1. Introduction

In recent decades, extracellular vesicles, especially exosomes, are attracting increasing attention for the vital functions in cellular transport and cell-cell communication (Mathieu et al., 2019). Exosomes, membrane-coated vesicles with a diameter of about 30–150 nm, are secreted by many types of eukaryotic cells *in vivo* (Hessvik and Llorente, 2018). Exosomes are involved in various normal physiological processes carrying complete bioactive molecules such as lipids, proteins, nucleic acids and metabolic components (Boriachek et al., 2018; van Niel et al., 2018). Exosomes are also found in several pathological processes implicated in neurodegenerative diseases and cancers (Gao et al., 2018; He et al., 2018; Yang et al., 2019a). Especially, exosomes are so-called "hallmarks of cancers" that participate in tumorigenesis, metastasis and drug resistance of tumors (Xu et al., 2018). Therefore, exosomes emerge as potent biomarkers of liquid biopsy and ideal candidates of drug delivery for early diagnosis, treatment and management of cancers. So far, exosome analysis mostly relies on differential centrifugation, western blotting, flow cytometry, ELISA and nano-particle tracking analysis (NTA) (Li et al., 2017; Ramirez et al., 2018; Wang et al., 2018). These methods have several disadvantages: some need expensive instruments and are lack of specificity, while others need a large number of samples. Given that the concentrations of exosomes in patients' fluids are extremely low at the early stages of diseases, it is of great importance to develop simple, sensitive, reliable and inexpensive methods for the sensing of exosome.

At present, immunomagnetic beads enables enrichment and separation of exosomes from complex body fluids through the interaction with surface markers, such as transmembrane superfamily members CD63 and CD81 (Jeong et al., 2016; Shao et al., 2018). However, since recognition element antibody as a type of protein is sensitive to external environment, the existing immunoassay is difficult to incorporate with signal amplification. On the other hand, thermally stable nucleic acid is frequently-used element in signal amplification for ultra-high efficiency and base-pairing precision (Deng et al., 2017; Wang et al., 2016; Zhao et al., 2015). Among them, isothermal nucleic acid amplification that avoids tedious thermal cycling of polymerase chain reaction (PCR) performs under near physiological condition, which is a suitable signal amplification strategy for biological analysis (Cai et al., 2018; Miao et al., 2015; Reid et al., 2018). Even so, dependence of polymerase and other tool enzymes not only increase analysis cost and operational instability, but also restrict kinetic rate of the amplification reaction (Chen et al., 2017). In 2000, Yurke et al. put forward a pioneering strand displacement reaction, in which a single DNA strand was enrolled in multiple cycles of DNA hybridization using toehold-mediated strand displacement reaction (TSDR) (Yurke et al., 2000). The enzyme-

* Corresponding author.
E-mail address: jingzhao@shu.edu.cn (J. Zhao).

https://doi.org/10.1016/j.bios.2019.111397
Received 2 April 2019; Received in revised form 22 May 2019; Accepted 31 May 2019
Available online 06 June 2019
0956-5663/ © 2019 Elsevier B.V. All rights reserved.

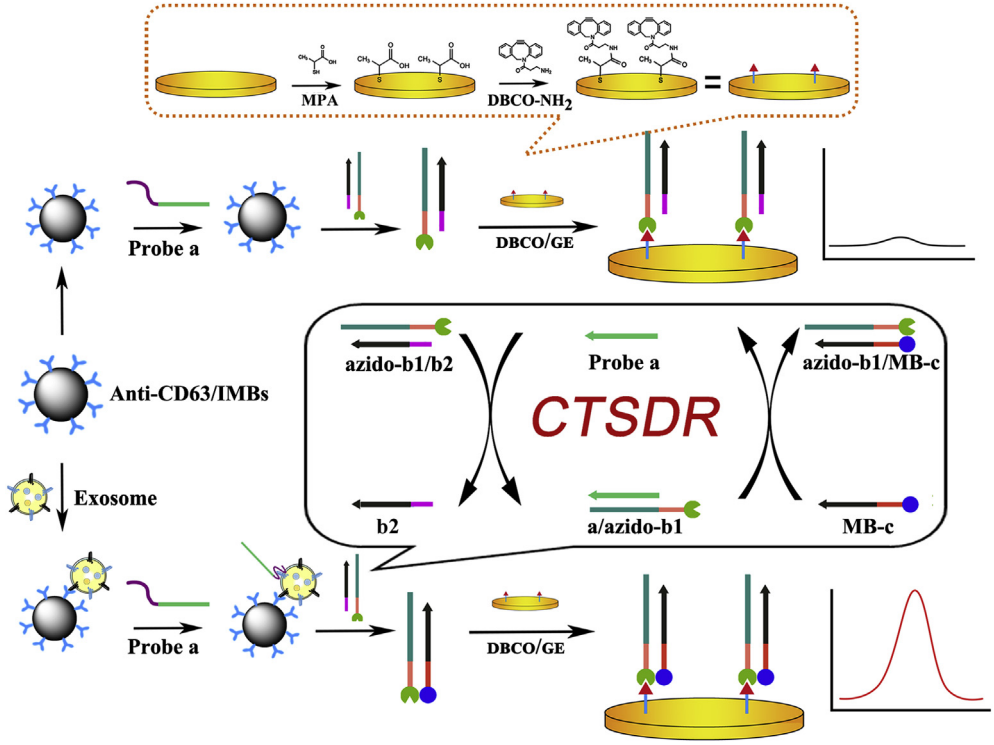

Scheme 1. Schematic illustration of amplified electrochemical detection of exosomes driven by a catalytic molecule machine.

free reaction performed under a mild condition and allowed kinetic control by varying length and sequence design of toehold. Later, a cascade TSDR (CTSDR) was proposed by using the output of strand displacement as the input of downstream reaction (Seelig et al., 2006). CTSDR not only eliminates continuous supplement of external triggers at each step, but also demonstrates 10^6 times faster reaction rates after input of external triggers (Lai et al., 2018; He et al., 2016; Yan et al., 2018). Considering that CTSDR is ultra-highly efficient autonomous system that has no specific requirement of external environment, we herein propose an amplified electrochemical method for quantitative sensing of exosomes by CTSDR-based catalytic molecule machine. To best of our knowledge, it is the first time to perform CTSDR on exosomes.

The principle of amplified electrochemical detection of exosomes is illustrated in Scheme 1. Generally, exosomes are firstly enriched on the surface of anti-CD63 antibody functionalized Immune Magnetic Beads (anti-CD63/IMBs) through the immune-recognition. A catalytic DNA chain, probe a, then binds to exosome using inherent CD63 aptamer region. After magnetic separation, probe a on exosome serves as a trigger to initiate catalytic molecule machine that relies on CTSDR. In a specific way, probe a reacts with the toehold of azido-b1 and thus releases b2 from azido-b1/b2 duplex. Newly formed a/azido-b1 exposes another toehold that is partially complementary to signal probe MB-c and thus initiate the displacement of probe a to produce a new duplex azido-b1/MB-c. Released probe a immediately triggers a new cycle of displacement of b2 from azido-b1/b2. After multiple cycles of CTSDR, a large number of azido-b1/MB-c duplexes are generated as the products of molecule machine. Because azido-b1 and MB-c are modified with azide and methylene blue groups, respectively, azido-b1/MB-c duplex can be transferred onto a dibenzocyclooctyne (DBCO)-functionalized gold electrode (DBCO/GE) which are prepared according to our previous work (Wang et al., 2019) and generate amplified electrochemical signals. Since the catalytic molecule machine is only be initiated with the input of external triggers from the recognition of exosomes, sensitive electrochemical sensing of exosomes is achieved by tracing electrochemical responses of CTSDR products-introduced MB.

2. Experimental section

2.1. Chemicals and materials

ExoEasy Maxi Kit was purchased from Qiagen Inc. (Hilden, GER). Carboxylated magnetic beads, 3,3′-dioctadecyloxacarbocyanine perchlorate (DIO) and streptavidin-phycoerythrin (SA-PE) were purchased from Invitrogen (Shanghai, China). Anti-CD63 antibody was purchased from Abcam (Shanghai, China). Mercaptopropionic acid (MPA), mercaptohexanol, N-hydroxysuccinimide (NHS), N-(3-Dimethylaminopropyl)-N′-ethlcarbodiimide hydrochloride (EDC), bovine serum albumin (BSA) and DBCO-amine (DBCO-NH_2) were obtained from Sigma-Aldrich (Shanghai, China). HepG2 and MCF-10A cells were purchased from the Institute of Biochemistry and Cell Biology of Chinese Academy of Science (Shanghai, China). Dulbecco's modified Eagle medium (DMEM) and fetal bovine serum (FBS) were purchased from Biological Industries Co., Ltd. (Shanghai, China). Normal human serum was obtained from AmyJet Scientific Inc. (Wuhan, China). All solutions were prepared with Milli-Q water (18.2 MΩ cm^{-1}) from a Milli-Q purification system (Milford, USA). All other chemicals were of analytical reagent grade. All DNA probes used in this research were synthesized and purified by Shanghai Sangon Biotechnology Co., Ltd. (Shanghai, China). Their sequences were listed in Table S1 in Supporting Information.

2.2. Cell culture and exosome isolation

HepG2 and MCF-10A cells were cultured in DMEM medium supplemented with 10% FBS in a humidified incubator at 37 °C with 5% CO_2 and 80% relative humidity. Exosomes were isolated from the supernatant media of the two cell lines. To this end, cells were cultured in conventional media contained 10% FBS to 70–80% confluence and then washed twice with phosphate-buffered saline (PBS), followed by incubation for 48 h in serum-free medium. Afterward, the culture medium was centrifuged at 4 °C (800 × *g* for 5 min and 2000 × *g* for 10 min) to remove intact cells or cellular debris and filtered through a

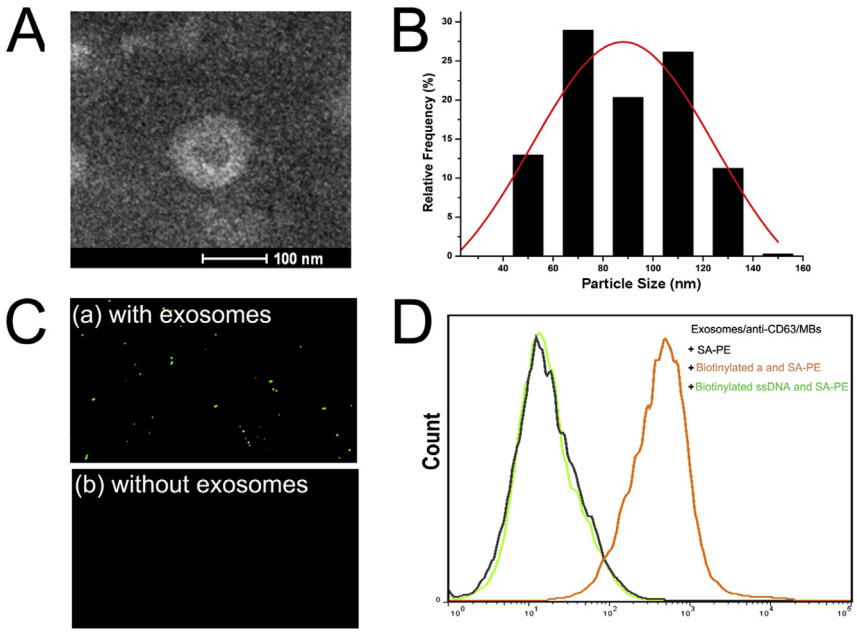

Fig. 1. (A) TEM image and (B) NTA analysis of exosomes isolated from culture medium of HepG2 cells. (C) Fluorescence images of anti-CD63/IMBs dyed with DIO which were (a) incubated or (b) not incubated with target exosomes. (D) Flow cytometry analysis of captured exosomes recognized by biotinylated a or random ssDNA and then stained by SA-PE. A control group without recognition by biotinylated a or random ssDNA indicated the background.

0.22 μm filter to discard large contaminating vesicles. Finally, exosomes were isolated from the culture medium using ExoEasy Maxi Kit according to manufacturer's instructions.

2.3. Validation of CTSDR using gel electrophoresis analysis

For gel electrophoresis, 10 μL of DNA samples (a, b2, c, b1/b2, a/b1, b1/c, b1/b2 incubated with a, b1/b2 incubated with c and the CTSDR mixture of a, b1/b2 and c) were first prepared, followed by being incubated with 2 μL of 6 × loading buffer. Afterward, the samples were subjected to a 10% non-denaturing polyacrylamide gel (PAGE) in 1 × Tris-borate-EDTA buffer. Electrophoresis separation was then running at a constant voltage of 120 V for 90 min. After being stained with SYBR Green I for 30 min, the resulting gel was photographed with a GelDoc XR$^+$ System (Bio-Rad, USA).

2.4. Electrochemical detection of exosomes driven by the catalytic molecule machine

Prior to exosome detection, anti-CD63/IMBs were prepared by attaching the antibody to carboxylated magnetic beads. Briefly, carboxylated magnetic beads were first washed three times with 100 μL of PBS and then activated with 0.22 M EDC and NHS for 30 min. After magnetic separation, the beads were mixed with 50 μL of the anti-CD63 antibody and incubated for 30 min at room temperature with gentle rotation. After being blocked with 0.1% BSA, the anti-CD63/IMBs were separated from the mixture with the aid of magnet, washed three times with PBS and finally resuspended in PBS before use.

A typical experiment for electrochemical detection of exosomes was performed by firstly mixing 25 μL of anti-CD63/IMBs and 25 μL of different concentrations of exosomes at 37 °C for 1 h. Thereafter, the magnetic beads were separated and further reacted with 25 μL of 0.1 μM probe a to sustain interaction between CD63 aptamer region and CD63 protein on exosome surface for 0.5 h. After being washed three times with PBS, the beads were further mixed with 50 μL of hybridization buffer containing 400 nM azido-b1/b2 and MB-c to conduct CTSDR at 4 °C for 20 min. Finally, the resulting supernatant liquid was obtained after magnetic separation and transferred onto a DBCO/GE which was prepared according to our previous work (Wang et al., 2019).

2.5. Electrochemical measurements

Electrochemical measurements were conducted on a CHI-660c electrochemical workstation (CH Instruments) with a conventional three-electrode system, consisting of a GE as the working electrode and a platinum wire electrode and saturated calomel electrode as the counter and reference electrodes, respectively. Electrochemical impedance spectra (EIS) were recorded by using $[Fe(CN)_6]^{3-/4-}$ as the redox probe and applying a bias potential of 0.224 V. Square wave voltammetry (SWV) responses were measured in the potential range from −0.35 to −0.05 V with 25-mV of amplitude by using Tris-HCl buffer as electrolyte. All measurements were conducted at least three times.

3. Results and discussion

3.1. Characterization of exosomes

Exosomes that are isolated from culture media of liver cancer cell line HepG2 are used as model in this work. Fig. 1A displays a typical TEM image of isolated exosome. Bilayer membrane-coated vesicle is shown with a diameter of about 110 nm, which is similar as that in other reports (Liu et al., 2018; Wang et al., 2017). Fig. 1B presents NTA result of exosomes, which confirms the size as that shown in TEM image. To validate immunobead-based capture of exosomes, anti-CD63/IMBs with or without incubation of target exosomes were dyed with a lipid phase marker, DIO. It could be seen that intense fluorescence was detected on the surface of MBs after incubating with target exosomes (Fig. 1C, a), while no observable fluorescence was detected on the surface of control IMBs in the absence of exosomes (Fig. 1C, b). The results clearly demonstrate the successful capture of exosomes on immunobeads. Fig. 1 D further reveal the binding of probe a to captured exosomes by flow cytometry. A biotinylated probe a and random ssDNA were designed as a signal output and a control, respectively. As shown in Fig. 1D, after biotinylated a bound to captured exosomes by virtue of CD63-aptamer recognition, SA-PE was recruited onto exosome surface through streptavidin-biotin interaction and thus aroused an obvious fluorescence signal. Instead, no signals were observed upon the absence of biotinylated a or using biotinylated ssDNA, indicating specific binding of probe a and exosome. Overall, TEM and NTA characterization confirmed the morphology of exosomes isolated from culture

medium of HepG2 cells, while fluorescence imaging and flow cytometry demonstrated sandwich-like structure consisting of anti-CD63/IMBs, HepG2-derivated exosome and probe a.

3.2. Validation of CTSDR

As the core of catalytic molecule machine used for exosome detection, CTSDR was first investigated via gel electrophoresis. Fig. S1 in Supporting Information shows PAGE results of stepwise reaction involved in CTSDR by using probe a as an input in the solution environment. Lane 2–7 (from left to right) exhibited the bands of a, b2, c, b1/b2, a/b1 and b1/c in sequence. When probe a mixed with b1/b2, single-stranded part of b1/b2 that was complementary to a served as a toehold to initiate strand displacement reaction. As a result, b2 was released from b1/b2 and a new duplex a/b1 was formed (Lane 8). When b1/b2 was mixed with c, c was inactive that could not react with b1/b2 for lack of toehold region. In this sense, c and b1/b2 were identical with their original conditions (Lane 9). When probe a, b1/b2 and c coexisted, probe a reacted with b1/b2 to form a new duplex a/b1 while c reacted with a/b1 to form b1/c and released probe a to trigger next round of strand displacement. As a result of CTSDR, large amounts of b1/c duplexes were produced (Lane 10). The results are consistence with our expectation and also conform to our principle.

We also used fluorescence spectrum to reconfirm the feasibility of CTSDR. To this end, we designed a FAM-labeled b1 (b1-F) and a Dabcyl-labeled b2 (b2-Q). Fig. 2A shows fluorescent signals in the case of different DNA strands. A quite low fluorescent intensity was observed at the wavelength of 522 nm in the presence of b1-F/b2-Q, ascribing to the active quench of fluorescence signals resulted from simple DNA hybridization (curve a). When both b1-F/b2-Q and c were added, low fluorescent intensity was similar as that in the presence of only b1-F/b2-Q (curve b), because c could not react with b1-F/b2-Q at an inactive state. Curve c represented slight increase of fluorescent intensity in the presence of both a and b1-F/b2-Q, suggesting the separation of fluorophore and quencher from stand displacement. However, only a small amount of a/b1 complex were generated upon a “one-to-one” relationship without recycling of a at a low concentration. Unlike the others, a significantly enhanced fluorescent intensity was observed in the presence of a, b1-F/b2-Q and c, demonstrating high efficiency of CTSDR (curve d). In addition, as shown in Fig. 2B, CTSDR was demonstrated in a time-dependent manner, as fluorescent intensity increased over time (curve a). In contrast, unspecific reaction of b1/b2 and c were at a quite low reaction rate, as only a slight increase of background signal was observed (curve b). Overall, fluorescent studies validated high rationality of CTSDR in our method.

3.3. Catalytic molecule machine-driven electrochemical biosensing of exosomes

Having confirmed its feasibility, we then transferred CTSDR into a catalytic molecule machine and used for the sensing of exosome. For this purpose, DBCO/GE was prepared to link CTSDR with electrochemical techniques. EIS, which is able to effectively reflect interface properties of a modified electrode, was used to verify stepwise preparation of DBCO/GE. As shown in Fig. 3A, nearly no impedance was observed at a bare electrode, proving feasible electron transfer between electrochemical probe molecule potassium ferricyanide and the electrode (curve a). Slight increases of impedances were observed after functionalization with MPA and subsequent linking with DBCO, which were ascribed to its electrostatic repulsion and hydrophobic nature (curve b and c). With the help of click chemistry, azido-b1/c duplex covalently attached to the DBCO/GE surface by using azido group of b1. In this case, substantial increase of negative charges strongly repelled potassium ferricyanide, leading to significant increase of impedance value (cure d). Overall, EIS studies first demonstrated the successful preparation and usability of DBCO/GE. Fig. 3B further reveals electrochemical responses incorporated with molecule machine. In the presence of probe a, azido-b1/b2 and MB-c, cycles of CTSDR were carried out by recycling of probe a and a large amount of azido-b1/MB-c duplexes were thus produced. Azido-b1/MB-c duplexes were subsequently captured onto DBCO/GE and generated a high SWV response for the approaching of MB to electrode surface (curve a). By contrast, an extremely low SWV response was observed in the presence of azido-b1/b2 and MB-c, indicating ultra-low displacement efficiency without external triggers (curve b). In addition, nearly no SWV responses could be observed in the presence of a, b1/b2 and MB-c or only MB-c, both of which reconfirmed the capture by making use of click chemistry (curve c and d). Overall, SWV results clearly revealed that CTSDR could be easily connected to electrode surface to yield a catalytic molecule machine.

In order to demonstrate high efficiency of catalytic molecule machine, we compared the concentration-dependent SWV responses in two types of strand replacement reaction, CTSDR and TSDR. Fig. S2 shows electrochemical responses by using CTSDR and TSDR in the presence of different concentrations of probe a. For CTSDR, peak current increased with the concentration of probe a from 5 pM to 1 nM, and a saturated peak current of ~2.5 μA was obtained with the addition of 1 nM probe a (Fig. S2A). For TSDR that did not involve recycling of probe a, peak current increased with the concentration of probe a from 2.5 to 600 nM, and a similar saturated peak current of ~2.5 μA was obtained with the addition of 600 nM probe a, 600 times greater than that in CTSDR (Fig. S2B). The comparison demonstrated high efficiency of recycling of probe a involved in catalytic molecule machine, laying the foundation for highly sensitive electrochemical biosensing.

Encouraged by these attractive features, we proceeded to employ

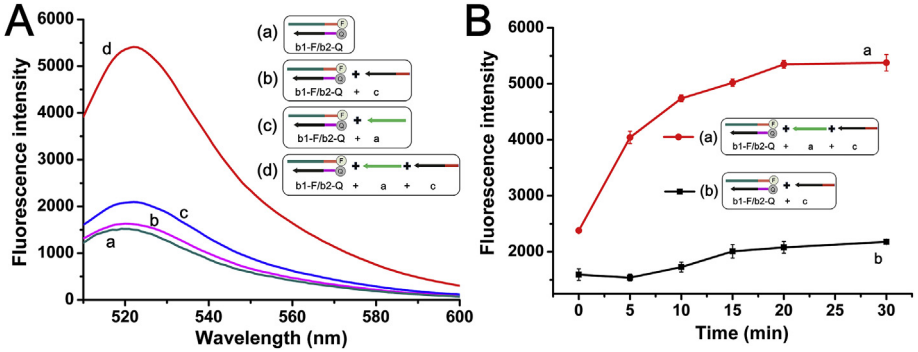

Fig. 2. (A) Fluorescence validation of CTSDR in the case that (a) b1-F/b2-Q, (b) b1-F/b2-Q and c, (c) b1-F/b2-Q and a and (d) b1-F/b2-Q, a and c were added, respectively. (B) Changes of fluorescent intensities over time in the presence of (a) b1-F/b2-Q, a and c or (b) only b1-F/b2-Q and c.

catalytic molecule machine to electrochemically detect exosomes. Beforehand, several optimized experiments were conducted to achieve an ideal performance. Fig. S3 shows optimization result of reaction time for CTSDR, from which we could see that peak current gradually increased with reaction time and reached the plateau after 20 min. Therefore, optimal reaction time for CTSDR was chosen as 20 min. The time consumption of the CTSDR was minimum with respect to DNA technologies (e.g., 60 min for rolling circle amplification, 30 min for DNA nanotetrahedra, and 80 min for exonuclease III-aided signal amplification) used in reported exosome detection methods (Dong et al., 2018; Huang et al., 2018; Wang et al., 2017), and thus may improve the detection efficiency. Fig. S4 shows electrochemical responses obtained upon using different concentrations of azido-b1/b2 for CTSDR. Peak current increased with the concentration of azido-b1/b2 from 25 to 400 nM and tended to be stable after then. Therefore, 400 nM was chosen as the optimal concentration of azido-b1/b2. The most appropriate reaction time for click chemistry was also explored. As shown in Fig. S5, reaction time increased from 2.5 min to 30 min, while peak current gradually increased and reached plateau after 15 min. So, 15 min was asserted to be the optimal reaction time for click chemistry. Under theses optimal conditions, a series of different concentrations of exosomes were detected. It could be seen from Fig. 3C that with the increase of exosome concentration, SWV responses from surface-attached MB increased, correspondingly. The result is reasonable, because enhanced amount of exosomes leads to increase of probe a recruited onto the surface of immunobeads, and thus greatly accelerate the efficiency of CTSDR to facilitate the generation of azido-b1/MB-c duplexes for signal obtaining. Fig. 3D shows the relationship between peak current and exosome concentration. The peak current gradually increased with exosome concentration in the range of 0–1 $\times$ 10^8 particles/mL. The inset further shows a good linear relationship between the peak current and the logarithm of exosome concentration from 1 $\times$ 10^5 to 5 $\times$ 10^7 particles/mL with a regression equation of I (μA) = $-2.682 + 0.599$ lg*Cexosome* (particles/mL) (R^2 = 0.998). The detection limit is calculated to be 1.72 $\times$ 10^4 particles/mL defined at 3 signal-to-noise ratio, which is better than most existing detection methods (Table S2). The experiments at each concentration were repeated at least five times with an average RSD of 2.8%, indicating good repeatability of our method.

To verify the clinical usability of our method, exosomes from a non-tumorigenic cell line MCF-10A were chosen as a control group. As shown in Fig. 4A, a quit low electrochemical response was obtained in the absence of exosomes (curve a), while relatively higher electrochemical responses were obtained in the presence of exosomes (curve b and c). At the meanwhile, peak current of HepG2-derived exosomes was higher than that of MCF-10A-derived exosomes, indicating a distinct expression level of CD63. These data are in accordance with reported literature, revealing that our method is capable of distinguishing exosomes secreted by cancer cells (Jin et al., 2018; Yang et al., 2019b). Moreover, serum tests were conducted to examine the performance of our method in complex environment. As shown in Fig. 4B, HepG2-derived exosomes with a concentration of 5 $\times$ 10^6 particles/mL and 5 $\times$ 10^7 particles/mL were diluted into PBS buffer and 10% ultra-centrifugation FBS (UC FBS), respectively. Ideally, the two kinds of samples produced signals with no significant difference ($p > 0.05$), indicating satisfactory anti-interference performance of our method. In addition, normal human serum (10%) without or with addition of HepG2-derived exosomes were also tested by our method. Experimental results revealed that the exosomes could be detected in human serum samples with good accuracy, suggesting the potential use of our method in clinical practice.

4. Conclusions

To sum up, we established an amplified electrochemical biosensing method for the detection of exosomes by using a catalytic molecule machine. In this method, a sandwich-like structure is first formed, consisting anti-CD63/IMBs, exosome and probe a that contained aptamer region of CD63. Surface-attached probe a is able to serve as external triggers and thus initiate the catalytic molecule machine. With the recycling of probe a, a large amount of signal duplex is produced and transferred to electrode surface by a fast click chemistry reaction. The use of antibodies and aptamer ensures high specificity in recognition and enrichment of exosomes, while signal amplification from the catalytic molecule machine greatly improves the detection sensitivity. In this sense, our method can be effectively applied in complex serum

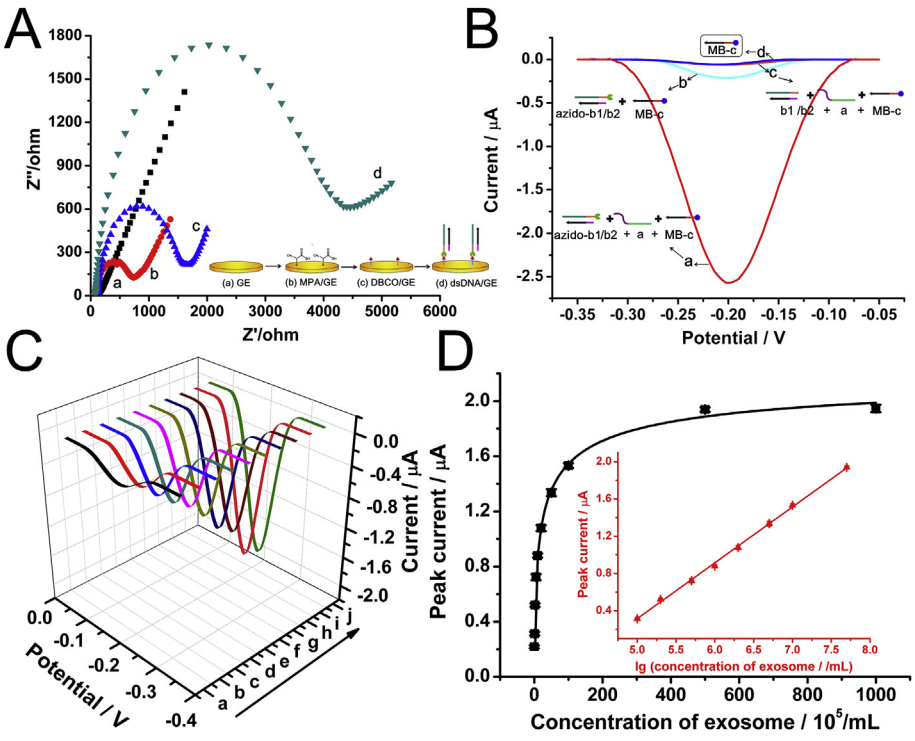

Fig. 3. (A) Nyquist diagrams obtained at (a) bare GE, (b) MPA-modified GE (MPA/GE), (c) DBCO/GE and (d) DBCO/GE reacted with azido-b1/c. Electrolyte: 5 mM $[Fe(CN)_6]^{3-/4-}$, biasing potential: 0.224 V. (B) SWV responses obtained in the presence of (a) probe a, azido-b1/b2 and MB-c, (b) azido-b1/b2 and MB-c, (c) probe a, b1/b2 and MB-c and (d) only MB-c. (C) SWV responses of different concentration of HepG2-derivated exosomes. From a to j: 0, 1 $\times$ 10^5, 2 $\times$ 10^5, 5 $\times$ 10^5, 1 $\times$ 10^6, 2 $\times$ 10^6, 5 $\times$ 10^6, 1 $\times$ 10^7, 5 $\times$ 10^7 and 1 $\times$ 10^8 particles/mL. (D) The relationship between peak current and exosome concentration. Inset shows a linear relationship between the logarithm of exosome concentration and peak current from 1 $\times$ 10^5 to 5 $\times$ 10^7 particles/mL.

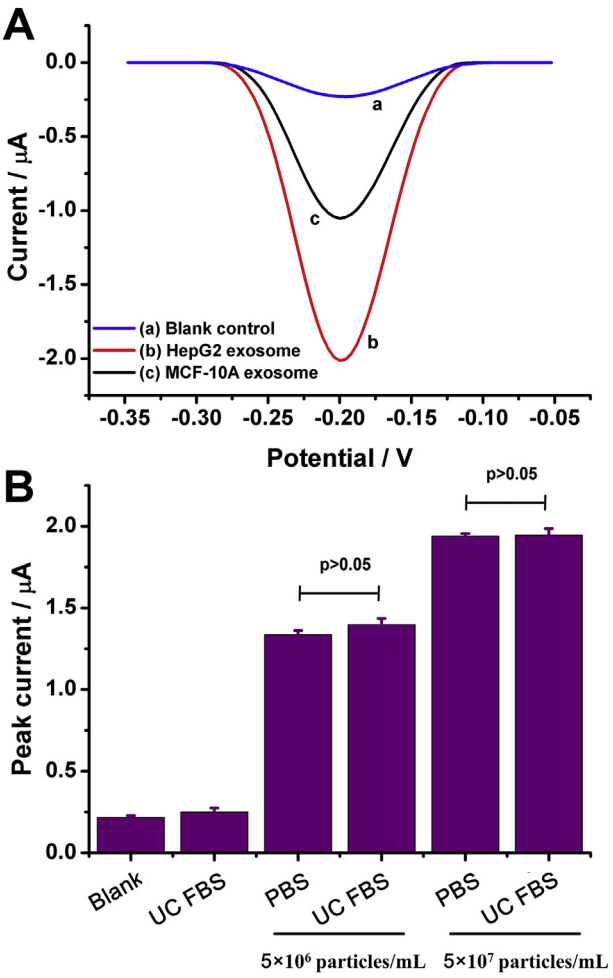

Fig. 4. (A) SWV responses for detection of (a) no exo-some, (b) 1×10^8 particles/mL HepG2-derived exosomes and (c) 1×10^8 particles/mL MCF-10A-derived exosomes. (B) SWV peak currents obtained upon analyzing blank control, 10% UC FBS, 5×10^6 particles/mL HepG2-derived exosomes in PBS and 10% UC FBS, and 5×10^7 particles/mL HepG2-derived exosomes in PBS and 10% UC FBS.

samples and suggested potential application in clinical samples. Certainly, our method still has some limitations. For example, the method may fail at the discrimination of subpopulations of exosomes because the CD63 is a common exosomal transmembrane protein. Nevertheless, the rapid development of aptamer selection techniques may provide opportunities to solve this issue. In the future, by making use of aptamers that are able to specifically bind to a certain type of exosomes, our method can be extended to distinguish exosomes from different sources. This may be critical to early diagnosis of cancers in clinic and is an ongoing subject of interest in our lab.

Declaration of interests

The authors declare that they have no known competing financial interests or personal relationships that could have appeared to influence the work reported in this paper.

CRediT authorship contribution statement

Ya Cao: Writing - original draft, Writing - review & editing. **Lingling Li:** Formal analysis, Writing - review & editing. **Bing Han:** Formal analysis, Writing - review & editing. **Ying Wang:** Writing - review & editing. **Yuhao Dai:** Writing - review & editing. **Jing Zhao:** Supervision, Writing - original draft, Writing - review & editing.

Acknowledgments

This work was supported by the National Natural Science Foundation of China (Grant Nos. 81871449, 81671781 and 31200745).

Appendix A. Supplementary data

Supplementary data to this article can be found online at https://doi.org/10.1016/j.bios.2019.111397.

References

Boriachek, K., Islam, M.N., Moller, A., Salomon, C., Nguyen, N.T., Hossain, M.S.A., Yamauchi, Y., Shiddiky, M.J.A., 2018. Small 14, 1702153.
Cai, S., Jung, C., Bhadra, S., Ellington, A.D., 2018. Anal. Chem. 90, 8290–8294.
Chen, J., Tang, L., Chu, X., Jiang, J., 2017. Analyst 142, 3048–3061.
Deng, R., Zhang, K., Li, J., 2017. Acc. Chem. Res. 50, 1059–1068.
Dong, H., Chen, H., Jiang, J., Zhang, H., Cai, C., Shen, Q., 2018. Anal. Chem. 90, 4507–4513.
Gao, L., Wang, L., Dai, T., Jin, K., Zhang, Z., Wang, S., Xie, F., Fang, P., Yang, B., Huang, H., van Dam, H., Zhou, F., Zhang, L., 2018. Nat. Immun. 19, 233–245.
He, C., Zheng, S., Luo, Y., Wang, B., 2018. Theranostics 8, 237–255.
Hessvik, N.P., Llorente, A., 2018. Cell. Mol. Life Sci. 75, 193–208.
He, X.W., Zeng, T., Li, Z., Wang, G.L., Ma, N., 2016. Angew. Chem. Int. Ed. 55, 3073–3076.
Huang, L., Wang, D.B., Singh, N., Yang, F., Gu, N., Zhang, X.E., 2018. Nanoscale 10, 20289–20295.
Jeong, S., Park, J., Pathania, D., Castro, C.M., Weissleder, R., Lee, H., 2016. ACS Nano 10, 1802–1809.
Jin, D., Yang, F., Zhang, Y., Liu, L., Zhou, Y., Wang, F., Zhang, G.J., 2018. Anal. Chem. 90, 14402–14411.
Lai, W., Ren, L., Tang, Q., Qu, X., Li, J., Wang, L., Li, L., Fan, C., Pei, H., 2018. ACS Nano 12, 7093–7099.
Li, P., Kaslan, M., Lee, S.H., Yao, J., Gao, Z., 2017. Theranostics 7, 789–804.
Liu, C., Xu, X., Li, B., Situ, B., Pan, W., Hu, Y., An, T., Yao, S., Zheng, L., 2018. Nano Lett. 18, 4226–4232.
Mathieu, M., Martin-Jaular, L., Lavieu, G., Thery, C., 2019. Nat. Cell Biol. 21, 9–17.
Miao, P., Tang, Y., Wang, B., Yin, J., Ning, L., 2015. Trac. Trends Anal. Chem. 67, 1–15.
Ramirez, M.I., Amorim, M.G., Gadelha, C., Milic, I., Welsh, J.A., Freitas, V.M., Nawaz, M., Akbar, N., Couch, Y., Makin, L., Cooke, F., Vettore, A.L., Batista, P.X., Freezor, R., Pezuk, J.A., Rosa-Fernandes, L., Carreira, A.C.O., Devitt, A., Jacobs, L., Silva, I.T., Coakley, G., Nunes, D.N., Carter, D., Palmisano, G., Dias-Neto, E., 2018. Nanoscale 10, 881–906.
Reid, M.S., Le, X.C., Zhang, H., 2018. Angew. Chem. Int. Ed. 57, 11856–11866.
Shao, H., Im, H., Castro, C.M., Breakefield, X., Weissleder, R., Lee, H., 2018. Chem. Rev. 118, 1917–1950.
Seelig, G., Soloveichik, D., Zhang, D.Y., Winfree, E., 2006. Science 314, 1585–1588.
van Niel, G., D'Angelo, G., Raposo, G., 2018. Nat. Rev. Mol. Cell Biol. 19, 213–228.
Wang, M., Tang, Y., Chen, Y., Cao, Y., Chen, G., 2019. Anal. Chim. Acta 1045, 77–84.
Wang, S., Zhang, L., Wan, S., Cansiz, S., Cui, C., Liu, Y., Cai, R., Hong, C., Teng, I.T., Shi, M., Wu, Y., Dong, Y., Tan, W., 2017. ACS Nano 11, 3943–3949.
Wang, W., Luo, J., Wang, S., 2018. Adv. Healthc. Mater. 7, 1800484.
Wang, Z., Li, Y., Han, P., Mao, X., Yin, Y., Cao, Y., 2016. Chem. Commun. 52, 10684–10687.
Xu, R., Rai, A., Chen, M., Suwakulsiri, W., Greening, D.W., Simpson, R.J., 2018. Nat. Rev. Clin. Oncol. 15, 617–638.
Yurke, B., Turberfield, A.J., Mills Jr., A.P., Simmel, F.C., Neumann, J.L., 2000. Nature 406, 605–608.
Yan, N., Wang, X., Lin, L., Song, T., Sun, P., Tian, H., Liang, H., Chen, X., 2018. Adv. Funct. Mater. 28, 1800490.
Yang, B., Chen, Y., Shi, J., 2019a. Adv. Mater. 31, 1802896.
Yang, Y., Li, C., Shi, H., Chen, T., Wang, Z., Li, G., 2019b. Talanta 192, 325–330.
Zhao, Y., Chen, F., Li, Q., Wang, L., Fan, C., 2015. Chem. Rev. 115, 12491–12545.